

Selection of Efficient Inhibitors for Caspas-9 according to Structure-Based Pharmacophore Screening Strategy and Molecular Dynamics Simulations

Samira Ansari^{a,b*}, Ali Naghi Kamali^a, Kowsar Bagherzadeh^b, Masoud Amanlou^b, Sajjad Aghabalazadeh^{a,c}

^a *CinnaGen Medical Biotechnology Research Center, Alborz University of Medical Sciences, Karaj, Iran.*

^b *Department of Medicinal Chemistry, Faculty of Pharmacy and Pharmaceutical Sciences Research Center, Medical Sciences, University of Tehran, Iran.*

^c *Center of Excellence in Electrochemistry, Faculty of Chemistry, University of Tehran, Tehran, Iran.*

Article history:

Received: 22 September 2017

Accepted: 25 October 2017

Keywords:

Alzheimer's disease

Caspase-9

Docking

Inhibitor

Pharmacophore

Virtual screening

HIGHLIGHTS

- Caspase-9 is an important enzyme for apoptosis and its activity is pivotal in cell death.
- A computational design of small molecular inhibitors for caspase-9 performed by structure-based pharmacophore model.
- 9 compounds from both National Cancer Institute (NCI) and ZINC databases were discovered as potent inhibitors.

ABSTRACT

Caspases are enzymes which are the main pathways for apoptosis. Any irregularity in their functions causes increase or decrease in cell death, which result in autoimmune disease or cancer, respectively. In this study, structure-based pharmacophore drug discovery method as a virtual screening was used to discover selective inhibitors for caspase-9. This enzyme is an initiator caspase that is the main pathway in Alzheimer's disease. A pharmacophore model was developed by investigating essential interactions among the reported potent inhibitors employing a docking analysis methodology. Applying pharmacophore virtual screening, nine compounds from both National Cancer Institute (NCI), and ZINC databases were filtered as potent inhibitors of caspase-9. The efficiency of the discovered compounds was further investigated by docking studies.

Introduction

Apoptosis is a programmed cell death which is a crucial process in development, maintenance of cell homeostasis, and regulation of immune system. When the apoptosis is either excessive or insufficient, it could result in many disease including cancer, autoimmune disease, viral

infection, and neurological disorders (Rudel, 1999; Talanian et al., 2000).

In mammalian, apoptosis is activated throughout three main pathways by caspase enzymes whose names are given from their ability in the cleavage of substrates after an Asp residue (Shi, 2002): extrinsic (death receptor pathway), intrinsic (apoptosome pathway), and cytotoxic lymphocyte-initiated granzyme B pathway (Cullen and Martin, 2009). In extrinsic and intrinsic pathways, apoptosis is driven by caspases from initiators (caspase-8, 9) to effectors (caspase-3, 7). Thus, activation

* Corresponding Author:
E-mail: @cinnagen.com

and inhibition of initiator caspases is a central regulatory step in cellular physiology (Shi, 2005) and has made caspases considerable targets to design cytoprotective drugs. Also, the inhibition of excessive apoptosis is considered as the main ways to treat or reduce signs of disease (Yaoita et al., 1998; Braun et al., 1999; Cursio et al., 1999; Schulz et al., 1999; Lee et al., 2000; Mocanu et al., 2000).

Oxidative damage, by aging and disease, leads to mitochondria dysfunction, releasing cytochrome C and then it activates Caspase-9 continued by effectors caspases (Rohn et al., 2002). There are some evidences confirming that the cleavage of Asp421 by caspases is more rapid in tau cleavage, so caspases activation could hyperphosphorylate tau proteins and have effective roles in the cleavage of amyloid precursor protein (APP), and tau protein (Rohn and Head, 2009; Rohn, 2010). Enhancement in tau proteins increases neurofibrillary tangles (NFTs) (Rohn et al., 2002).

Extracellular plaques of amyloid- β and intercellular neurofibrillary tangles (NFTs) are defined in Alzheimer's disease as a progressive disorder (Chong et al., 2005). Since caspase-cascade is a very effective pathway for apoptosis (Denault and Salvesen, 2002; Shiozaki et al., 2003), in this study caspase-9 inhibition was investigated. Caspase-9 belongs to caspases initiator class, which is activated by death stimulus in upstream. So, its inhibition causes stopping cell death during the caspase cascade (Cohen, 1997; Denault and Salvesen, 2002; Philchenkov, 2004).

Caspases have a special recognition sequence including at least four N-terminal amino acids in their active site (Rudel, 1999; Grutter, 2000). Active site in caspase-9 is recognized by a four amino acid sequence (LEHD) involving an aspartic acid residue in the P1 position and a small hydrophobic residue in the P2 position, in CARD domain from caspase-3, 7, and then by limited proteolysis change of them to active forms (Rudel, 1999; Grutter, 2000; Renatus et al., 2001; Yang et al., 2003; Yoshimori et al., 2007)

Structure-based pharmacophore model generating from the optimal interactions of already experimentally reported inhibitors with the target macromolecular is defined as a very helpful method for screening a ligand database and more effective inhibitor models. Then, the obtained information enable medicinal chemists to develop molecules with higher binding affinities for the target macromolecule and can be used to generate specific biological responses (Yoshimori et al., 2007).

In this study, a computational design was performed for selection of small molecular inhibitors against Caspase-9 by developing and modifying a pharmacophore model based on tripeptidyl inhibitor (PHQ-GLU-VAL-ASP), which is recrystallized in the Protein Data Bank file (pdb code 1jxq) by employing docking strategy.

Materials and Methods

Enzyme structure preparation

Enzyme caspase-9 structure file was obtained from RCSB Protein Data Bank (pdb code, 1jxq, 2.80 Å) (Shiozaki et al., 2003; Philchenkov, 2004). The pdb structure was refined due to a large missing part in the crystallographic structure. This missing sequence contained 35 amino acids (ASTSPEDESPGSNPEPDATPFQEGLRTFDELDAIS). Homology modeling strategy was applied to fix the large gap in the structure. Since there was no crystallographic structure with an acceptable similarity to that of caspase-9 by complete amino acid sequencing, caspase-9 structure was found by blasting the enzyme sequence employing the online program BLAST from NCBI. Then, it was decided to solely perform homology model with the missing part. The target sequence was aligned to those with similar sequence to identify appropriate templates for the subsequent homology modeling procedure. MODELER 9.10 (Sali and Blundell, 1993) employed four structures with PDB IDs of 4DGE, 4DGA, 2PBj, and 1Z9H as the appropriate templates to build the missing part structure of caspase-9. While the obtained structure mainly contains loops and turns, an α -helix (DELDAIS) and a β -sheet (ASTS) were also observed. This structure was linked to that of the crystallographic one with the aid of Hyperchem 8.0 and then, GROMACS MD package 4.5.5 and GROMOS96 53ab as classical molecular dynamic simulations (MDs), using for minimizing and optimizing of energy and also an appropriate structure was achieved after 40 nanoseconds of MDs (Fig. 1).

The Ramachandran plot of the enzyme average structure during the equilibration state was plotted (Fig. 2). Obviously, only 4 amino acids of the modeled sequence are in the forbidden region and two out of four are Gly that can be present in both regions. Therefore, the obtained overall enzyme was employed for the rest of the study.

Docking methodology

Autodock tools 1.5.4 were used for preparing input files. The grid maps were calculated and the docking procedure was performed by Auto grid 4.2 and Auto dock 4.2, respectively. Ligands docked on Caspase-9 were those from binding database, reported until August 2012 (Liu et al., 2007).

The grid box of 126, 126, 126 Å (x, y and z) as the large grid box and 66, 66, 68 Å (x, y and z) as the small grid box were assigned on caspase-9 binding pocket with the spacing of 0.375 Å. Other docking study parameters were as follow: number of Lamarckian job=100; initial population =100; maximum number of energy evaluation =25×105; maximum generations =27000; mutation rate

Table 1. Details of the best ligands elicited from pharmacophore search based on docking studies. (Abbreviations; LS: Ligand Scout, hyd: hydrophobic, acc: acceptor, aro: aromatic, don: donor, pos: position). Structure of ligands were depicted in figure 4.

Ligand	Binding Energy	LS pharmacophore feature	H-bond contacts	MW	xlogP ^a
2a	-9.29	3 hyd, 2 acc, 1 aro	Arg 335, Gly 238, Cys 287	409	6.26
2b	-6.89	3 hyd, 3 acc	Arg 355, Arg 180, Cys 287, Ser 353, Gly 238	397.441	4.05
2c	-7.12	4 hyd, 2 acc, 1 aro	Thr 181	454.448	4.14
2d	-7.19	2 hyd, 1 acc	Arg355, Arg 180	484.474	4.20
2e	-7.08	3 hyd, 1 acc	Tyr 251	460.477	4.51
2f	-6.88	4 hyd, 2 acc, 1 aro	Arg 180, Tyr 251	479.458	3.90
2g	-6.30	5 hyd, 1 acc	Arg 355	438.471	3.43
2h	-6.63	3 hyd, 1 acc, 1 don	Arg 355, Glu 290	483.49	5.38
2i	-6.85	1 hyd, 1 acc, 1 pos	Tyr 251	466.483	4.71

of 0.02.; a crossover rate of 0.80.

Pharmacophore model generation and virtual screening

Structure based pharmacophore model approach was used for considering the ligands modes of interactions in the protein binding pocket. LigandScout v.301 software was employed for development and refinement of all pharmacophore models (Wolber and Langer, 2005). The obtained models were then used as filters during the virtual screening by Ligandscout v.301 to extract ligands with desired pharmacophore features from NCI and ZINC compound databases (each compound in its 25 conformers).

Classical molecular dynamic simulations

GROMACS MD package 4.5.5 and GROMOS96 force field are reinforced for classical molecular dynamic simulations (Pronk et al., 2013). PRODRG server was applied to obtain the ligand's topology files (Schuttelkopf and van Aalten, 2004). The initial structure that contained caspase-9 in complex with the target ligand in their best mode of interaction according to the calculated binding energy and orientations in the binding pocket was derived from the former docking studies. The desired complex was immersed in a dodecahedron-shaped box (X, Y and Z) with minimum distance of 1nm from each edge of the box, while, periodic boundary conditions were also

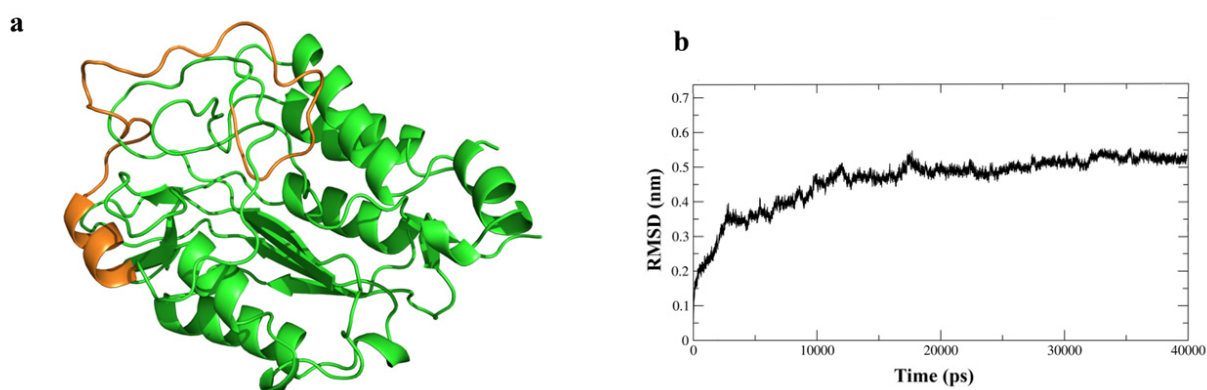


Figure 1. a. The protein structure after classical molecular dynamic simulations, the target sequence is shown in orange color, **b.** The backbone root mean square deviations (RMSD) plot of the enzyme during 40 nanoseconds of simulations.

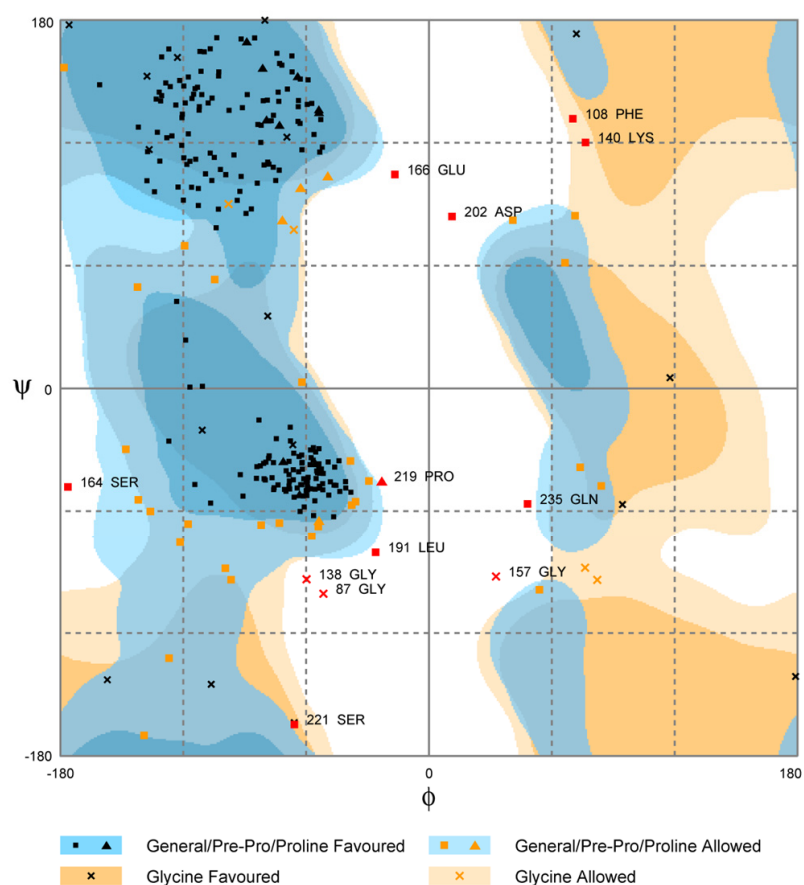


Figure 2. The Ramachandran plot of the enzyme average structure during the equilibration state, the filled red color points represent the target sequence residues.

assigned in all directions. Some Na^+ counter ions were substituted by water molecules randomly to neutralize the system net charge. Steepest descent algorithm was employed to minimize energy of system. The system went through NVT ensemble MD simulations for 20ps right after convergence, followed by simulations under NPT ensemble at 300 K. Berendsen barostat and thermostat were used to keep the pressure and temperature constant at 1 bar and 300 K. The partial mesh Ewald method was used to calculate long-range electrostatic interactions. For restraining, the bond lengths LINCS was employed with an integration step of 1 fs. The MD simulations were extended NPT for 10 nanoseconds at constant pressure and temperature conditions.

Data analysis and presentation software

LigandScout v3.01, Autodock tools 1.5.4, Discovery studio v3.5 and PyMOL software were used to analyze and visualize all ligand-protein interactions. PyMOL was

also employed to better illustrate ligand-proteins modes of interactions for MD simulations studies.

Results and Discussion

Docking studies and model creation

For validation of docking method in the best docked conformation, RMSD (root mean square deviation) extracted from experimental, should be $<2.0 \text{ \AA}$, then, the used scoring function is acceptable (Wang et al., 2003). In our validation, RMSD value was excellent for the native ligand, which was 0.623 \AA .

A Structure-based pharmacophore model was generated according to a three amino acid peptide in the crystallised structure of the caspase-9 protein. The model was further modified according to the structure of the active pocket. In these structure-based generated models (models 2-pharmacophore) virtual screening resulted in 19 compounds to be considered as caspase-9 inhibitors. To specify more, docking by a small grid box on active site

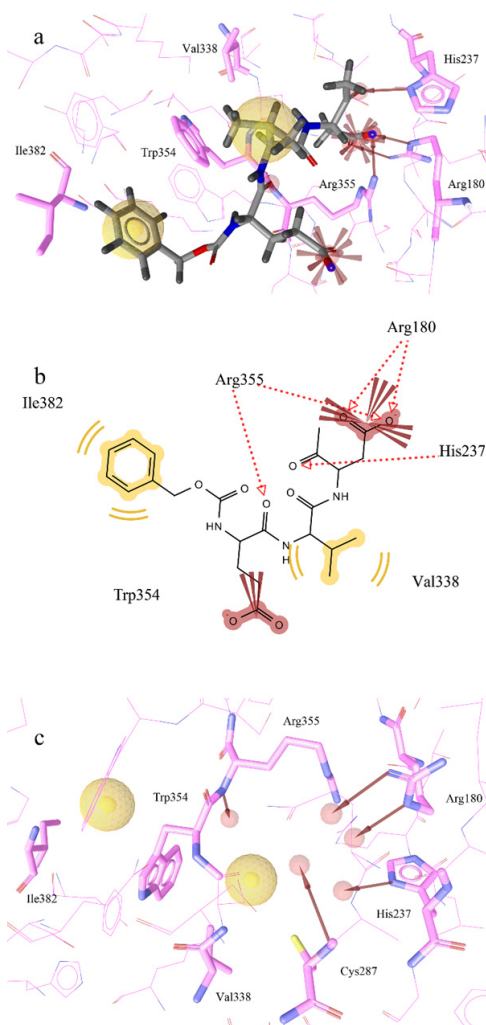


Figure 3. Pharmacophore model (model 1) generated from 1JXQ/ tripeptidyl sequence PHQ-GLU-VAL-ASP. a. red arrows; HBA, yellow spheres; hydrophobic sites, gray spheres; excluded volumes, and red stars; negative ionizable interactions. b. the pharmacophore model interactions with the active pocket residues. c. The modified pharmacophore model (model 2-pharmacophore), (red arrows; HBA, yellow spheres; hydrophobic sites, gray spheres; excluded volumes).

was done on 19 compounds in model 2-pharmacophore in which finally 9 compounds were achieved. The extracted compounds affinities were ranked by employing docking methodology. Rigid docking studies were carried out using Autodock 4.2, and the results are presented in Table 1.

Pharmacophore virtual screening is taken out on some compounds according to their similarity to the models and further continued by docking methodology to extract those with higher affinity for the active site. According to the docking studies results, models 2-pharmacophore

resulted in 9 compounds with considerable affinities for the active site. The proper compounds were chosen based on their docking binding energy value, drug like parameters, and also their orientation in the pocket. Among obtained compounds, 2a was selected as the best because of the best binding energy, including critical interaction by amino acids in active site of the receptor's pocket. Molecular dynamics was carried out on 2a as the best parameters to interact with caspase-9.

Protein crystallography structure includes two-chain caspase 9 which missed first 138 residue by proteolytic removal of the CARD. The crystal contains tripeptidyl inhibitor in active site (Renatus et al., 2001). It should also be mentioned that Arg 355, Arg 180, His 237, and Cys 287 are the key amino acids of the active pocket of enzyme caspase-9 as it was already reported in the literature (Renatus et al., 2001; Chao et al., 2005; Yoshimori et al., 2007). Further, hydrophobic and H-bonding interactions are the main contacts between the ligands and the active site.

The crystallographic structure and the peptide sequence in the active site were studied thoroughly and were used for pharmacophore model generation. Model 1-pharmacophore was generated focusing on the interactions of a tripeptidyl sequence PHQ-GLU-VAL-ASP trapped in the active pocket (Fig. 3.a). The model 1 included H-bond acceptors (red arrows) which showed that there were 4 H-bond acceptors via His237, Arg180, and Arg355 (Renatus et al., 2001; Chao et al., 2005; Yoshimori et al., 2007). Moreover, a hydrophobic area was created in Ile382, Trp354, and Val338 area. The two negative ionizable interactions occurred as a result of the carboxylate functional groups of the peptide amino acids (Glu and Asp).

By virtual screening of the database of the pharmacophore model 1-pharmacophore, no coincident structure with this model was obtained. Consequently, to broaden the applicability of the model, the number of pharmacophores was reduced by omitting the two negative ionizable pharmacophores. To more specify Model 2-pharmacophore, the techniques of structure-based pharmacophore modeling was used and a hydrogen bond acceptor pharmacophore with original position (Orig. Pos.) 23.80, 43.67, and -8.98, tolerance 1.5, and weight 1, was created through NH functional group of Cys287 (model 2-pharmacophore, Fig. 3.c).

Model 2-pharmacophore screening resulted in 19 compounds, after that, docking studies by a blind dock on active pocket, 9 compounds (2a-i, Fig. 4) were found to have better affinities and orientation to interact with the critical residues of the caspase-9 active site. The exact type of these compounds interactions and binding energies were further investigated. Docking procedure was repeated assigning small grid box on the active site, and the final results are reported in Table 1.

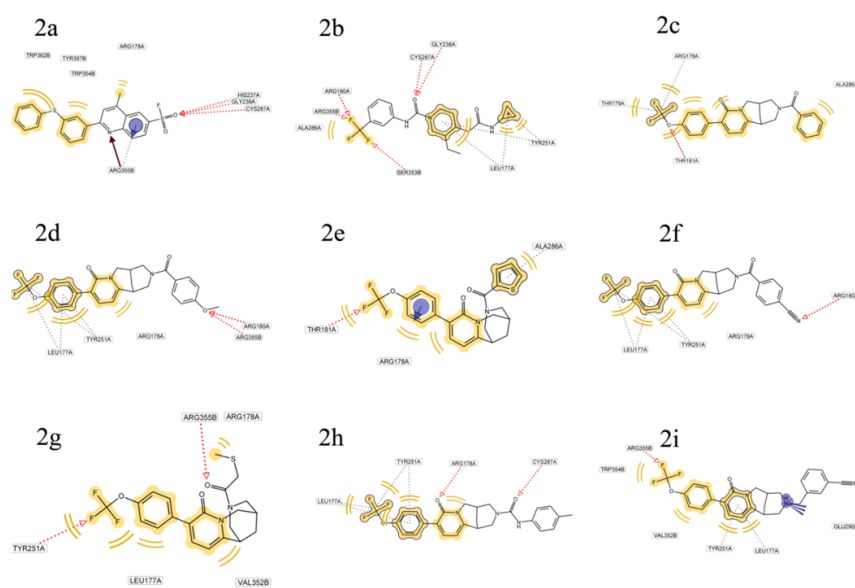


Figure 4. The compounds elicited from pharmacophore screening of model 1-pharmacophore (Fig. 1-c) after docking studies.

Molecular dynamic simulations

According to the calculated docking binding energy value and its modes of interactions, an appropriate conformation of the most potent ligand in complex with caspase-9 was obtained to be compound 2a.

The complex of compound 2a with caspase-9 was

assigned to classical molecular dynamic simulations to further evaluate the obtained binding pose stability and the ligands consistency in the active pockets in a dynamic environment while the solvent effects were also included. The backbone root mean square deviations (RMSD) of the protein backbone as well as the ligand itself were plotted with respect to their initial structure (the energy

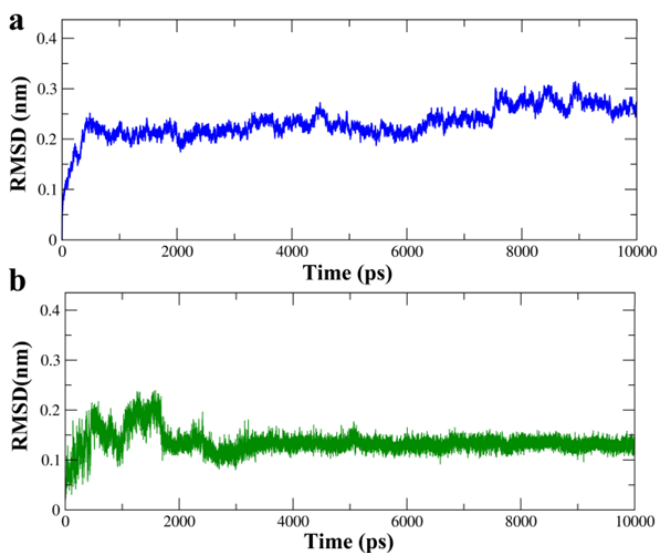


Figure 5. RMSD plots of **a.** Caspase-9 backbone in complex with ligand 2a (blue), and **b.** Ligand 2a backbone in complex with caspase-9, during 10 nanoseconds of MD simulations.

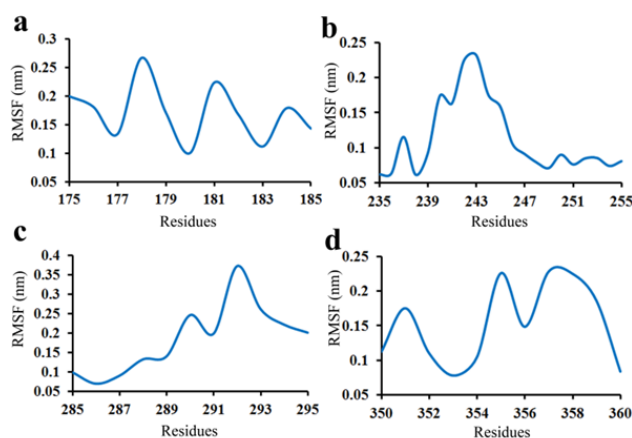


Figure 6. RMSF plots of caspase-9 residues in complex with ligands 2a, a. residues 175-185, b. residues 235-255, c. residues 285-395, d. residues 350-360.

minimized structure) and as a function of the simulation time to ensure the system reached the equilibration state. As it is shown in Fig. 5, no significant deviations were observed for both the protein backbone and the ligand which indicated the efficiency of the established interactions between them. In point of fact, while notable deviations were observed in the ligand conformation for the establishment of efficient interactions in caspase-9 binding pocket in the first 3 nanoseconds of the simulation time which then almost became fixed in its position, the protein did not need to go under significant conformational changes for the formation of a conducive binding.

Further, to better observe the enzyme residues behavior throughout MD simulations time, root mean square fluctuations (RMSF) of the amino acids were calculated and graphed. According to Fig. 4, residues Arg180, His237, Gly238, Tyr251, Ala286, Cys287, and Trp354 showed the least fluctuations because of their presence in the pliable parts of the protein, loop, and turn structures. This rigidity can be attributed to the involvement of the mentioned residues in interaction with the ligand. Also a very significant fluctuation was observed for residue Pro357 (Fig. 6) confirming that this residue has to change its orientations in order to establish better electrostatic interactions with the diphenyl sulfide fragment of the compound.

According to the results obtained via the performed molecular dynamic simulations, the compound stood firm in the binding pose was obtained from the docking studies and was stabilized in the pocket by the interactions discussed.

The studied ligand average position during 10 nanoseconds of MD simulations is shown in Fig. 7. Several hydrogen bonds were formed between

compound 2a and Arg180, Cys287, Arg355 and Trp354 (the red dashes). Also electrostatic interactions between diphenyl sulfide benzene rings, and residues Trp354 and Pro357 were quite inevitable. Further, the fluorophosphate fragment enabled several salt bridge formations as well.

The stability of the hydrogen bonds formed between the ligand and active pocket residues was computed as well. Based on Fig. 8, as the simulations progress, the hydrogen bonds number increases as well, showing that the dynamic nature of the simulations method gives the chance to both protein and the ligand to fit into their best conformations where they can conduct productive interactions. Also, this phenomenon provided more evidences the ligand stability in caspase-9 binding pocket.

The catalytic site structures of caspase-9 enzyme after energy minimization and 10 nanoseconds of MD simulations were superimposed to get a better insight of the impact of the dynamic environment of the modes of interactions. As it is presented in Fig. 9, the residues (Trp354, Pro357 and Arg355) orientations that are interacting with diphenyl sulfide fragment has changed dramatically as well as the conformation of the target fragment itself, but the mode of interactions (π - π electrostatic interactions) did not show any changes. In contrast, quinoline as well as fluorophosphate fragments seem to have stayed almost fixed in their positions due to the establishment of hydrogen bonds, salt bridges, and also protonated salt bridges that kept both the ligand, and the involved residues firm, as well as the rigid nature of this part of the ligands structure.

Conclusion

This study indicates that the combined structure-based pharmacophore drug discovery method, pharmacophore

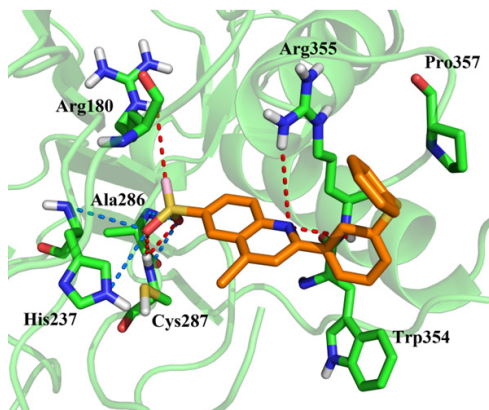


Figure 7. The studied ligands average positions in the active pocket, the red dashes represent hydrogen bonds and the blue dashes represent salt bridges.

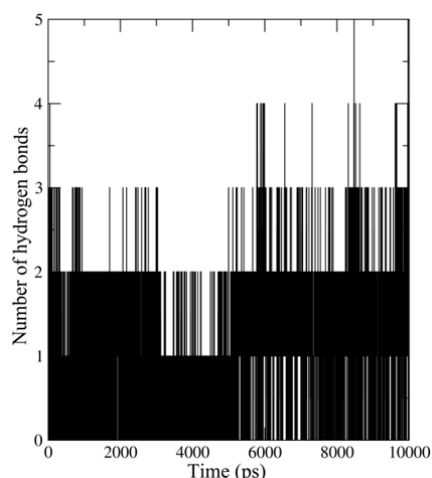


Figure 8. Number of hydrogen bonds evolution during 10 nanoseconds of simulations time.

virtual screening, and docking analysis methodology have been effective approaches for the identification and characterization of the potent inhibitors of caspase-9.

Acknowledgements

This study was supported by a grant from the Research Council of Tehran University of Medical Sciences.

Competing Interests

The authors declare that there are no conflicts of interest.

References

- Braun, J. S., Novak, R., Herzog, K. H., Bodner, S. M., Cleveland, J. L. and E. I. Tuomanen, (1999). "Neuroprotection by a caspase inhibitor in acute bacterial meningitis." *Nature Medicine*, 5(3): 298-302.
- Chao, Y., Shiozaki, E. N., Srinivasula, S. M., Rigotti, D. J., Fairman R. and Y. Shi, (2005). "Engineering a dimeric caspase-9: a re-evaluation of the induced proximity model for caspase activation." *PLOS Biology*, 3(6): e183.
- Chong, Z. Z., Li, F. and K. Maiese, (2005). "Employing new cellular therapeutic targets for Alzheimer's disease: a change for the better?" *Current Neurovascular Research*, 2(1): 55-72.
- Cohen, G. M. (1997). "Caspases: the executioners of apoptosis." *Biochemical Journal*, 326 (Pt 1): 1-16.
- Cullen, S. P. and S. J. Martin, (2009). "Caspase activation pathways:

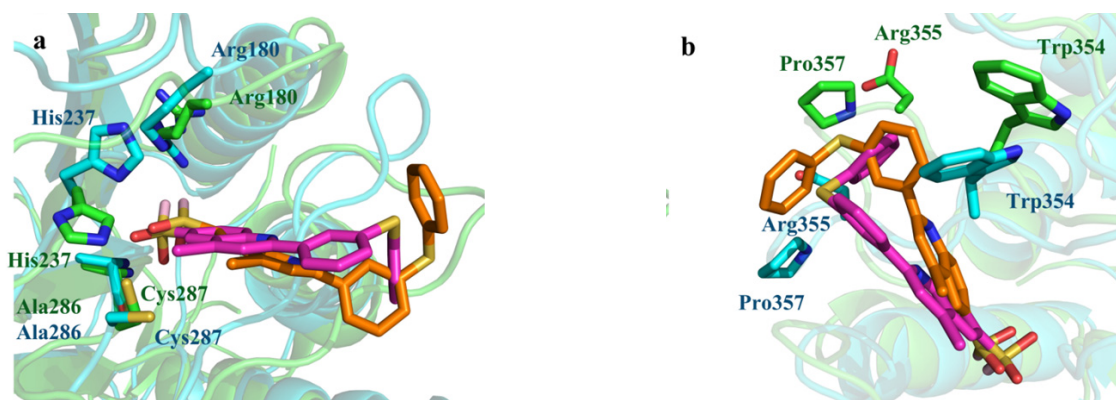


Figure 9. The superimposed structures of the energy minimized ligand-protein complex (ligand is shown in magenta and the protein in cyan) the one after 10 nanoseconds of MD simulations (ligand is shown in orange and the protein in green). To avoid complications, **a.** represents interactions of diphenyl sulfide fragment, and **b.** represents quinoline and fluorophosphate fragments.

some recent progress." *Cell Death & Differentiation*, **16**(7): 935-938.

Cursio, R., Gugenheim, J., Ricci, J. E., Crenesse, D., Rostagno, P., Maulon, L., Saint-Paul, M. C., Ferrua, B. and A. P. Auberger, (1999). "A caspase inhibitor fully protects rats against lethal normothermic liver ischemia by inhibition of liver apoptosis." *The FASEB Journal*, **13**(2): 253-261.

Denault, J. B. and G. S. Salvesen, (2002). "Caspases: keys in the ignition of cell death." *Chemical Reviews*, **102**(12): 4489-4500.

Grutter, M. G. (2000). "Caspases: key players in programmed cell death." *Current Opinion in Structural Biology*, **10**(6): 649-655.

Lee, D., Long, S. A., Adams, J. L., Chan, G., Vaidya, K. S., Francis, T. A., Kikly, K., Winkler, J. D., Sung, C. M., Debouck, C., Richardson, S., Levy, M. A., DeWolf, W. Keller, E., P. M., Tomaszek, T., Head, M. S., Ryan, M. D., Haltiwanger, R. C., Liang, P. H., Janson, C. A., McDevitt, P. J., Johanson, K., Concha, N. O., Chan, W., Abdel-Meguid, S. S., Badger, A. M., Lark, M. W., Nadeau, D. P., Suva, L. J., Gowen, M. and M. E. Nuttall, (2000). "Potent and selective nonpeptide inhibitors of caspases 3 and 7 inhibit apoptosis and maintain cell functionality." *Journal of Biological Chemistry*, **275**(21): 16007-16014.

Liu, T., Lin, Y., Wen, X., Jorissen, R. N. and M. K. Gilson, (2007). "BindingDB: a web-accessible database of experimentally determined protein-ligand binding affinities." *Nucleic Acids Research*, **35**(Database issue): D198-201.

Mocanu, M. M., Baxter, G. F. and D. M. Yellon (2000). "Caspase inhibition and limitation of myocardial infarct size: protection against lethal reperfusion injury." *British Journal of Pharmacology*, **130**(2): 197-200.

Philchenkov, A. (2004). "Caspases: potential targets for regulating cell death." *Journal of Cellular and Molecular Medicine*, **8**(4): 432-444.

Pronk, S., Pall, S., Schulz, R., Larsson, P., Bjelkmar, P., Apostolov, R., Shirts, M. R., Smith, J. C., Kasson, P. M., van der Spoel, D., Hess, B. and E. Lindahl, (2013). "GROMACS 4.5: a high-throughput and highly parallel open source molecular simulation toolkit." *Bioinformatics*, **29**(7): 845-854.

Renatus, M., Stennicke, H. R., Scott, F. L., Liddington, R. C. and G. S. Salvesen, (2001). "Dimer formation drives the activation of the cell death protease caspase 9." *Proceedings of the National Academy of Sciences USA*, **98**(25): 14250-14255.

Rohn, T. T. (2010). "The role of caspases in Alzheimer's disease; potential novel therapeutic opportunities." *Apoptosis*, **15**(11): 1403-1409.

Rohn, T. T. and E. Head, (2009). "Caspases as therapeutic targets in Alzheimer's disease: is it time to "cut" to the chase?" *International Journal of Clinical and Experimental Pathology*, **2**(2): 108-118.

Rohn, T. T., Rissman, R. A., Davis, M. C., Kim, Y. E., Cotman, C. W. and E. Head (2002). "Caspase-9 activation and caspase cleavage of tau in the Alzheimer's disease brain." *Neurobiology of Disease*, **11**(2):

341-354.

Rudel, T. (1999). "Caspase inhibitors in prevention of apoptosis." *Herz*, **24**(3): 236-241.

Sali, A. and T. L. Blundell, (1993). "Comparative protein modelling by satisfaction of spatial restraints." *Journal of Molecular Biology*, **234**(3): 779-815.

Schulz, J. B., Weller, M. and M. A. Moskowitz, (1999). "Caspases as treatment targets in stroke and neurodegenerative diseases." *Annals of Neurology*, **45**(4): 421-429.

Schuttelkopf, A. W. and D. M. van Aalten, (2004). "PRODRG: a tool for high-throughput crystallography of protein-ligand complexes." *Acta Crystallographica Section D: Structural Biology*, **60**(Pt 8): 1355-1363.

Shi, Y. (2002). "Mechanisms of caspase activation and inhibition during apoptosis." *Molecular Cell*, **9**(3): 459-470.

Shi, Y. (2005). "Activation of Initiator Caspases: History, Hypotheses, and Perspectives." *Journal of Cancer Molecules*, **1**(1): 9-18.

Shiozaki, E. N., Chai, J., Rigotti, D. J., Riedl, S. J., Li, P., Srinivasula, S. M., Alnemri, E. S., Fairman, R. and Y. Shi, (2003). "Mechanism of XIAP-mediated inhibition of caspase-9." *Molecular Cell*, **11**(2): 519-527.

Talanian, R. V., Brady, K. D. and V. L. Cryns, (2000). "Caspases as targets for anti-inflammatory and anti-apoptotic drug discovery." *Journal of Medicinal Chemistry*, **43**(18): 3351-3371.

Wang, R., Lu, Y. and S. Wang, (2003). "Comparative evaluation of 11 scoring functions for molecular docking." *Journal of Medicinal Chemistry*, **46**(12): 2287-2303.

Wolber, G. and T. Langer, (2005). "LigandScout: 3-D pharmacophores derived from protein-bound ligands and their use as virtual screening filters." *Journal of Chemical Information and Modeling*, **45**(1): 160-169.

Yang, W., Guastella, J., Huang, J. C., Wang, Y., Zhang, L., Xue, D., Tran, M., Woodward, R., Kasibhatla, S., Tseng, B., Drewe, J. and S. X. Cai, (2003). "MX1013, a dipeptide caspase inhibitor with potent in vivo antiapoptotic activity." *British Journal of Pharmacology*, **140**(2): 402-412.

Yaoita, H., Ogawa, K., Maehara, K. and Y. Maruyama (1998). "Attenuation of ischemia/reperfusion injury in rats by a caspase inhibitor." *Circulation*, **97**(3): 276-281.

Yoshimori, A., Sakai, J., Sunaga, S., Kobayashi, T., Takahashi, S., Okita, N., Takasawa, R. and S. Tanuma, (2007). "Structural and functional definition of the specificity of a novel caspase-3 inhibitor, Ac-DNLD-CHO." *BMC Pharmacology*, **7**: 8.

This open-access article distributed under the terms of the Creative Commons Attribution-NonCommercial 4.0 International License (CC BY-NC 4.0).